Ionic remodelling following myocardial infarction explains phenotypic variability in ECG and arrhythmic substrate but not in ejection fraction

Xin Zhou*[1], Zhinuo Jenny Wang*[1], Julia Camps[1], Jakub Tomek[1,2], Alfonso Santiago[3,4], Adria Quintanas[3], Mariano Vazquez[3,4], Marmar Vaseghi[5,6], Blanca Rodriguez[1]

* co-first authors

1 Department of Computer Science, University of Oxford, UK

2 Department of Pharmacology, University of California, Davis, CA, USA

3 Department of Computer Applications in Science and Engineering, Barcelona Supercomputing Centre (BSC), Barcelona, Spain

4 ELEM Biotech, Barcelona, Spain

5 UCLA Cardiac Arrhythmia Center, University of California, Los Angeles, CA, USA

6 Neurocardiology Research Center of Excellence, University of California, Los Angeles, CA, USA

Author contact details:

Dr Xin Zhou: xin.zhou@cs.ox.ac.uk

Dr Zhinuo Jenny Wang: jenny.wang@cs.ox.ac.uk

Professor Blanca Rodriguez: blanca.rodriguez@cs.ox.ac.uk

Oxford address:

Department of Computer Science, Wolfson Building, Parks Road, Oxford OX1 3QD, UK

ABSTRACT

Aims:

Sudden death after myocardial infarction (MI) is associated with electrophysiological heterogeneities and ionic remodelling, which are reflected as variable phenotypes. Low ejection fraction (EF) is used in risk stratification, but its mechanistic links with the post-MI electrophysiological heterogeneities are unknown. We aim to unravel how phenotypic ECG and EF variability in post-MI may be explained by the impact of ionic remodelling on spatio-temporal dispersion of repolarization using human biventricular electromechanical modelling and simulation.

Methods and Results:

Multiple post-MI ECG phenotypes observed clinically were investigated using multi-scale modelling and simulation, calibrated and evaluated using experimental and clinical data. Acute stage T-wave inversion was caused by delayed repolarization in the epicardial border zone (BZ), and Brugada phenocopy was generated by repolarization delay and activation failure in the BZ. Upright tall T-waves in chronic MI represented large repolarisation dispersion between BZ and surrounding tissue, which promoted ectopic propagation at fast pacing. T-wave morphology alternans were present at fast-pacing due to prolonged refractoriness in the mid-myocardium. Post-MI ionic remodelling reduced EF through inhibition of calcium transient amplitude, but the EF at resting heart rate was not sensitive to the extent of repolarisation heterogeneity and the risk of repolarisation abnormalities at fast pacing.

Conclusions:

In acute post-MI, ionic remodelling and its effect on refractoriness and propagation failure in the BZ have a strong impact on phenotypic ECG variability, whereas in chronic post-MI, the repolarisation dispersion across the BZ is crucial. T-wave and QT abnormalities are better indicators of repolarisation heterogeneities than EF in post-MI.

Keywords: acute myocardial infarction, chronic myocardial infarction, computational modeling and simulation, ECG, ejection fraction

INTRODUCTION

Sudden cardiac death in post-myocardial infarction (post-MI) patients is due to lethal arrhythmias in 50% of cases at both acute and chronic infarct stages[1,2]. Risk stratification is currently based on low left ventricular ejection fraction (LVEF)[3,4] to identify patients who need the implantation of defibrillator devices. However, only a very small subset of patients that suffer from sudden cardiac death are identified by low LVEF, and a significant number of sudden deaths occur in patients with relatively preserved LVEF[5]. The mechanistic link between LVEF and arrhythmic events is not clear, therefore, it is necessary to improve post-MI arrhythmic risk stratification through mechanistically driven biomarkers.

Various electrocardiogram (ECG) characteristics were suggested by clinical studies to be relevant to the arrhythmic risk of post-MI patients. Longer QT intervals have been associated with increased mortality as well as ventricular tachycardia and fibrillation for both the acute and chronic stages[6,7]. However, QT prolongation in single leads can be a reflection of reduced global repolarisation reserve, while the regional heterogeneity of repolarisation in different post-MI zones can be more crucial than the global reserve for the development of re-entrant waves. QT dispersion between 12-leads was proposed as a potential marker for electrophysiological heterogeneity[8]; however, it was found to have good specificity but low sensitivity[8]. Prolonged T-peak to T-end interval (Tpe) [9] and increased incidence of T-wave alternans[10] were also found to be useful risk predictors in post-MI patients. However, despite the promising outcomes of those clinical studies, the ECG-based risk predictors are not widely applied in the clinical evaluation of the need for implantable cardioverter-defibrillators [4,11].

A key factor that hinders the clinical utility of ECG biomarkers is the large variability in post-MI phenotypes, their progression from acute to chronic, and between different patients. Variability in QT prolongation[6,12,13] and post-MI ECG morphologies constrain the use of single biomarker thresholds as predictors. Furthermore, an important limitation of non-invasive ECG biomarkers is their inability to provide direct measurements of regional electrophysiological heterogeneity caused by scar and ionic remodelling, which is critical for the arrhythmic substrate.

Many experimental studies have investigated the underlying mechanisms of increased repolarisation dispersion in post-MI patients. Specifically, repolarisation dispersion increases after MI, due to ionic differences between the border zone (BZ) surrounding the scar and the remote zone (RZ) myocardium[14]. The BZ at the acute stage can be characterised by reduced sodium current (I_{Na}), L-type calcium current (I_{CaL})[15,16], and rapid and slow delayed rectifier potassium currents (I_{Kr} and I_{Ks})[17], as well as enhanced CaMKII activity[18] and gap junction redistribution[19,20]. After a period of scar healing, ionic remodelling may partially recover[21,22], but increased late sodium current (I_{NaL}), calcium-activated potassium and chloride currents (I_{KCa} and I_{ClCa}) were observed in the chronic BZ and RZ[23]. Post-MI ionic remodelling can cause conduction abnormalities, repolarisation abnormalities, as well as variable alterations in the action potential duration (APD), which act as substrates of ventricular tachycardia[24]. It is, however, unclear how various degrees of repolarisation dispersion affect ECG biomarkers, and LVEF used for risk stratification. Therefore, further studies are needed to bridge the gap between cellular electrophysiological characteristics and variable patient phenotypes post-MI.

Human based modelling and simulations of electrophysiology and mechanics have been shown useful in the prediction of post-MI arrhythmic risk and myocardial stress and

strain[25–27]. However, previous work concentrated on either electrophysiology or mechanics, while the crosstalk between the two is the key to understand the relationship between LVEF and arrhythmic risk. Human based electromechanical models can fill in this gap and provide more insights into the risk prediction and treatment optimisation for post-MI patients.

The main goal of this study is, therefore, to investigate how varying degrees of ionic remodelling explain the phenotypic variability in ECG and LVEF biomarkers observed in acute and chronic post-MI patients, through variations in spatial and temporal repolarisation abnormalities and dispersion and calcium transient abnormalities. We hypothesise that ECG abnormalities can be explained by activation abnormalities, dispersion of repolarisation, early after depolarisations (EADs) and alternans, while the LVEF will reflect predominantly calcium transient and structural abnormalities and are insensitive to the ionic remodellings that underpin ECG disease markers. Using novel electromechanical human biventricular simulations, we aim to identify biomarkers that are most relevant to repolarisation dispersions, thus facilitating post-MI risk stratifications to go beyond LVEF.

METHODS

Mechanistic modelling and simulation is able to encapsulate cardiac physiology and the laws of physics and chemistry through the use of mathematical descriptions. They can be used to identify mechanisms of disease. In this study, the three-dimensional biventricular heart is represented by a computational mesh constructed from magnetic resonance images and is populated by the cellular model. The cellular model uses ordinary differential equations to represent the key ionic currents, elements of calcium handling, and cellular contractility.

Human multi-scale ventricular electromechanical modelling and simulation: from ionic remodelling to ECG and LVEF

We constructed a human electromechanical simulation framework to enable the investigations of variable post-MI patient phenotypes, from ionic remodelling to body surface ECGs and pressure-volume (PV) loops (Figure 1A). The cardiac magnetic resonance (CMR)-based biventricular anatomical mesh (Figure 1B) was included in the torso for ECG simulations, as in [28]. Electrical propagation was simulated using the monodomain equation with orthotropic diffusion based on rule-based fields for fibre, sheet, and inter-sheet directions[29], and transmural and apex-to-base heterogeneities as in [30] (Figure 1B). Electrical stimulus via Purkinje-myocardial junctions was simulated by an endocardial fast-activation layer with root node locations to achieve realistic QRS complex morphologies simulated using a pseudo-ECG method at clinically standard lead locations on the torso (Figure 1C), as in [30]. In the non-infarcted normal zone (NZ), monodomain diffusivities were calibrated to achieve experimentally measured orthotropic conduction velocity of 67 cm/s, 30 cm/s, and 17 cm/s[31].

Since anterior infarction is very common and related to the worst prognosis[32,33], 75% transmurality of infarct was introduced to the anterior myocardial wall (Figure 1C), with scar and border zones taking up 12.4% and 11.7% of ventricular volume (or 15.8% and 15.0% of left ventricular volume), respectively. Electrophysiological remodelling was implemented to the border zone (BZ) and the chronic remote zone (RZ). In BZ and infarct zones, the diffusivities were calibrated to reproduce conduction slowing (one-third of the NZ conduction velocities).

To recapitulate organ-level electromechanics, the human-based ToR-ORd electrophysiological model[34] was coupled with human excitation-contraction and active tension Land model[35] (Figure 1E), with sheet active tension being set to 30% of fibre active tension. To reflect the enhancement of the calcium-activated potassium current in the chronic stage, this new current formulation was implemented (see SM1 for details of the additional current formulation). Post-MI remodelling of ionic currents in the BZ and chronic RZ was introduced based on experimental measurements at acute and chronic stages (Figure 1E).

Human biventricular mechanical model

Strongly coupled electromechanics with orthotropic passive mechanical behaviour and balance of linear momentum with inertial effects were achieved as in [28,36]. An elastic spring boundary condition was set on the epicardial surface, to simulate pericardial constraint, and the basal plane was fixed in space to prevent unphysiological tilting and expansion due to the unavailability of closed basal geometry. Pressure boundary condition on the left and right endocardial surfaces were controlled using a five-phased state machine, which has 1) active diastolic inflation followed by electrical activation and 2) isovolumic contraction, 3) ejection

coupled with two-element Windkessel aortic haemodynamics model, 4) isovolumic relaxation, and 5) passive inflation and relaxation, to produce pressure-volume (PV) loops[28]. The passive stiffness parameters were calibrated to achieve 53% LVEF in a control simulation (see Supplementary Material Table S2 and S3 for a list of calibrated parameters).

The active tension was set to zero in the scar to represent the myocyte damage, and the chronic passive stiffness parameters of the infarct region were increased 10-fold to mimic fibrotic scar formation as in [37]. For each acute post-MI phenotype, a case of complete loss of contractile function (zero active tension) in the BZ was also simulated to evaluate the contribution of other non-ionic remodelling-related abnormalities on ejection fraction.

Experimentally-informed populations of post-MI electromechanical models

To account for the inter-subject electrophysiological variability widely observed in clinic, the baseline cellular electromechanical model was extended to populations of NZ models, and post-MI ionic remodelling was applied to generate population of post-MI models (Figure 1D). In addition to the baseline model, several representative cellular models were selected from the population and implemented into the biventricular electromechanical simulations.

An initial population of human ventricular cell models was constructed based on the ToR-ORd model by varying the conductances or magnitudes of I_{Na}, I_{NaL}, I_{to}, I_{CaL}, I_{Kr}, $I_{Ks,}$ I_{K1}, I_{NaCa}, I_{NaK}, J_{rel} and J_{up} by up to ±50% using Latin Hypercube Sampling. As illustrated in previous studies, small populations of models with proarrhythmic ionic remodelling achieved similar predictability as large populations with uniform current variations[38,39]. Therefore, we chose to start with a small NZ population (n=500) and then introduce multiple combinations of ionic remodelling to mimic the large post-MI variability. After calibration with human

experimental data[40,41] and discarding those manifesting EADs at 1Hz, 245 sets of endocardial, midmyocardial and epicardial models were accepted as the NZ population.

Several models of post-MI ionic remodelling were introduced to the NZ population to generate BZ and RZ populations for both acute and chronic post-MI, and they were constructed and evaluated based on experimental measurements, as described in Supplementary Materials Table S4. For acute post-MI (within a week post-occlusion), three types of BZ remodelling (Acute BZ1-3) were considered based on previous modelling work and experimental canine data collected within 5 days post-MI[25,42–44]. For chronic post-MI, ionic remodelling measured from minipigs 5 months post-MI with heart failure were used to generate Chronic BZ (affecting only the BZ) and Chronic RZ1 (also affecting the remote myocardium). Another type of remodelling, Chronic RZ2, was established based on multiple experimental data from failing human cardiomyocytes[45–56]. Furthermore, reduction of sodium current[46] and SERCA[47], with enhanced CaMKII activity and slower calcium release [57,58] were also implemented in Chronic BZ, RZ1 and RZ2, as observed in human failing cardiomyocytes. Both human recordings and animal data were used for model evaluation, given the scarcity of human tissue, summarised in Supplementary Material Table S5-S6.

Simulation protocols and biomarker calculation

Single virtual cardiomyocytes were paced at 1Hz for 500 beats to detect EAD generation. For alternans generation, single cells were paced at cycle lengths (CLs) of 500 ms, 400 ms and 300 ms for 500 beats, and a ΔAPD greater than 3 ms between the last two beats at steady state was defined as alternans.

Biventricular electromechanical simulations were performed at 800 ms CL (75 beats per minute) with 100 ms allowed for active diastolic filling prior to endocardial activation for each beat. For chronic post-MI, and baseline for comparison, an additional fast pacing protocol was applied with 500 ms CL (120 beats per minute), with 50 ms allowed for active diastolic filling for each beat. Three beats were sufficient to achieve stable ECG and PV characteristics at 800 ms CL, and six beats for 500 ms CL (see Figures S3~S5 for ECGs for all beats).

Clinical biomarkers were quantified from the simulated ECG (including the QT interval, QRS duration, T-wave duration, T peak to T end duration, T onset to T peak duration, and QT dispersion, see definition and method of evaluation in SM4), as well as from the simulated PV loop (including end diastolic and end systolic volumes, peak systolic pressures and LV and RV ejection fractions), as well as the wall thickening strain (see Table S5-S6 for ECG and PV biomarkers for all simulated beats).

Simulation software and computational framework

Cellular electrophysiological simulations and Latin Hypercube Sampling were performed using bespoke MATLAB codes. Coupled cellular electromechanics, as well as biventricular electromechanics simulations, were performed using the high-performance numerical software, Alya, for complex coupled multi-physics and multi-scale problems[59] on the CSCS (Swiss National Supercomputing Centre) Piz Daint supercomputer multi-core clusters, granted through the PRACE (Partnership for Advanced Computing in Europe) project.

RESULTS

Human multi-scale modelling and simulation reproduced ECG phenotypes in acute and chronic post-MI stages

Our multi-scale electromechanical simulations with experimentally calibrated ionic remodelling reproduced clinically reported ECG phenotypes (Figure 2) in patients at acute and chronic stages of post-MI [60–62]. When imposing acute post-MI remodelling, we reproduced T-wave inversion, Brugada phenocopy ST-segment elevation and QT interval prolongation in the anterior leads (Figure 2A), which are common ECG phenotypes observed in acute post-MI patients[60–62]. Our simulations were also able to recapitulate ECG morphology similar to healthy subjects with upright T-waves (Figure 2A, right), which can also characterise acute post-MI [61,62].

In chronic post-MI, our ECG simulations demonstrated upright T-waves, and global prolongations of QT intervals in all precordial leads (Figure 2B, top row), which are characteristic of chronic patients with worse clinical outcomes [6,7]. A range of T-wave durations were present, as can be found in chronic post-MI (Figure 2B, bottom row)[61,62].

T-wave inversion and Brugada phenocopy can indicate reversed transmural repolarisation gradient and activation failure in acute MI

We can now explain the ECG phenotypes identified for post-MI through the analysis of simulations and with reference to the specific ionic remodelling considered in each model. The inverted T-wave ECG phenotype was associated with a reversed transmural repolarisation gradient (Figure 3A, repolarisation time map insets), due to prolonged APDs in the epicardial BZ (Figure 3B, membrane potential). These APD prolongations originated

at the cellular level due to the BZ remodelling, which inhibited multiple potassium currents in the BZ (Figure 3C, the first column of I_{Kr}, and Supplementary Material Table S4 Acute BZ1).

The Brugada phenocopy ECG phenotype was due to regions of activation failure in the epicardial border zone (Figure 3A, the activation and repolarisation time maps), as well as a small region of delayed repolarisation in the near-apical portion of the border zone (Figure 3B, membrane potential). These were caused by strong inhibitions of sodium, calcium and potassium ionic currents in the border zone (Figure 3C, the second column of I_{Na}, I_{CaL}, I_{Kr}, and Supplementary Material Table S4 Acute BZ2).

Acute MI with upright T-waves corresponded to a comparable transmural repolarisation gradient as the control (Figure 3A, the repolarisation time map). In this case, the lack of potassium current inhibition accounted for the lack of ECG manifestations (Figure 3C, the third column of I_{Kr}, and Supplementary Material Table S4 Acute BZ3).

Variable T-wave width in chronic post-MI ECG can be explained by the extent of repolarisation dispersion between border zone and remote zone

In the chronic stage, global QT prolongation was due to APD prolongation in the remote myocardium (Figure 4, repolarisation time maps and membrane potentials). Recovery of the upright T-wave in the anterior leads (compared to the acute stage) was due to a recovery of the transmural repolarisation gradient (Figure 4A, the repolarisation time maps), given the milder I_{Kr} inhibition in the border zone (Figure 4C, the first column of I_{Kr}, and Supplementary Material Table S4 Chronic BZ). Furthermore, T-wave duration in this stage was mainly determined by the gradient between remote and border zone repolarisation times

(Figure 4A, repolarisation time maps), where more severe APD prolongation in the RZ led to larger repolarisation gradients and, consequently, larger T-wave duration and amplitude (Figure 2B).

LVEF failed to indicate the extent of post-MI repolarisation dispersions

In our simulations, acute MI ionic remodelling yielded mildly reduced LVEF (43% to 47%) compared with control (53%) (Figure 5A). LVEF reductions were caused by contractile dysfunction (Figure 5A, active tension) due to lowered calcium amplitude in BZ (Figure 3C, intracellular calcium transient), which was directly caused by inhibitions of I_{CaL} in all acute phenotypes (Figure 3C, I_{CaL}, and Supplementary Material Table S4). A complete loss of contractile function in the BZ resulted in a more severe reduction in LVEF in acute post-MI (40% for all acute phenotypes in Supplementary Material Figure S5).

Activation failure in Brugada phenocopy caused loss of contractility in the affected regions in the BZ (Figure 3A, activation and repolarisation time maps) and resulted in a more severely reduced LVEF with a substantial non-contracting region with significant wall thinning (Figure 5A, systolic wall thinning). Acute MI with no observable ECG abnormalities can still have reduced mechanical function, as measured by LVEF (Figure 5A, the last column). Comparison between this phenotype and the inverted T-wave phenotype shows that the mechanical dysfunction can be dissociated from repolarisation gradient and T wave abnormalities.

Chronic post-MI simulations showed mild reduction in peak systolic pressure (by 1 kPa) and some reduction in LVEF (Figure 5B), which were unaffected by differences in repolarisation gradients. This is because there is a consistent reduction in calcium transient

amplitude in the remote zone that is independent of the extent of APD prolongation (Figure 4, intracellular calcium transient and membrane voltage). Therefore, both the acute and chronic electromechanical simulation results showed the post-MI repolarisation dispersions do not affect the LVEF.

T-wave alternans and abnormal wave propagation are caused at fast pacing by cellular alternans and EADs, without reduced LVEF at resting heart rate

Increased incidence of T-wave alternans is commonly observed in post-MI patients, and abnormal propagation waves generated from post-MI electrophysiological heterogeneity can trigger lethal arrhythmic events. In the population of post-MI cellular models, higher inducibility of alternans was observed at both acute and chronic stages at fast pacing (Supplementary Material Figure S6). There were two origins of alternans in the population of models: classical calcium-driven alternans, predominantly observed in the epicardial population of models (Supplementary Material Figure S10), and EAD-driven alternans due to strong calcium current in midmyocardial cells (Supplementary Material Figure S11). The underlying calcium-driven mechanisms include the enhanced CaMKII activity and slower calcium release, as well as suppressed SERCA pump activity in the chronic stage, which are consistent with previous studies [63–66]. I_{KCa} enhancement in the chronic stage suppressed alternans generation (detailed analysis provided in Supplementary Material SM6). The median of calcium amplitude was larger in the alternans models than in the non-alternating post-MI models (Supplementary Material Figure S15), suggesting alternans models may present as a preserved LVEF.

Introducing a representative cellular alternans model in the biventricular modelling and simulation framework reproduced alternans in T-wave morphology as in post-MI patients. Figure 6 shows upright T-wave morphology and preserved LVEF of 49% at resting rate of 75 bpm (CL= 800 ms). However, at a fast pacing rate of 120 bpm (CL = 500 ms), significant beat-to-beat ST and T-wave morphology alterations were observed. This was due to large alternans in the midmyocardium of remote zone at CL of 500 ms (Figure 6B, fast pacing simulation column), with EAD-driven alternans. These results support the importance of stress tests, since cellular level alternans can be reflected as T-wave alternans rather than reductions of resting LVEF. This is consistent with reports that T-wave alternans under supine bicycle exercise testing was found to be predictive of arrhythmic event after acute post-MI[67].

In addition to alternans, EADs were also promoted in the population of chronic models versus acute models, due to less I_{CaL} inhibition in the chronic stage (Figure 7A, left, Supplementary Material Table S4). The key underlying combinations of ionic remodelling for EAD generation include the inhibition of I_{Kr}, the enhancement of I_{NaL}, which facilitate reactivation of I_{CaL} (Supplementary Material SM7). Similarly, the cellular models that showed EADs also had larger calcium amplitude (Supplementary Material Figure S23), suggesting a preserved LVEF.

In Figure 7, we investigate how cellular EADs contribute to arrhythmic wave generations in the ventricle at chronic stage post-MI (Figure 7A). At fast pacing (120 bpm), the epicardial remote zone cell model displayed EADs, whereas endo- and midmyocardium cell models exhibited repolarisation failure/alternans (Figure 7A, right). When placed into whole-ventricular simulations at fast pacing (Figure 7B), this caused abnormal wave

propagations. By the end of the first heartbeat (500 ms), the anterior epicardial BZ was fully repolarised, but the RZ showed EADs. This mean that after the second beat stimulus, at 610 ms (Figure 7B), the long APD of the RZ prevented full activation in the postero-lateral LV (Figure 7B, green and purple marker) while the BZ APD was shorter than RZ (Figure 7B, red marker) and so could be fully activated. This led to a significant membrane potential gradient between the BZ (red marker) and RZ (green marker) at 610 ms, leading to ectopic wave generation due to electronic effects at 710 ms in the boundary between BZ and RZ (Figure 7C, compare red and green traces). This ectopic wave propagated in an anti-clockwise fashion when viewed from the base from 810 to 910 ms (Figure 7B, basal view). In the right ventricle at 610 ms, incomplete repolarization caused a smaller action potential to be elicited by the sinus stimulus (Figure 7C, yellow trace), thus allowing successful propagation of the ectopic wave from the left to the right ventricle from 910 ms to 1010 ms (Figure 7B).

The simulated clinical biomarkers (Figure 7D) showed that while at a resting heart rate of 75 bpm (800 ms CL), our simulations produced preserved LVEF of 49%, and prolonged QT interval of 669 ms (Figure 7D, resting simulation), at fast pacing the abnormal simulated ECGs reflected the underlying ectopic wave propagation (Figure 7D, fast pacing simulation) with a loss of coordinated mechanical function. This episode illustrates that large APD dispersion between BZ and RZ can become the trigger of ectopic wave propagation due to electrotonic gradients. The prolonged global QT interval with large T-wave duration and amplitude in leads facing the infarct can be indicative of such risk, while the LVEF can be preserved at rest.

DISCUSSIONS

In this study, the key characteristics and variability of ECG phenotypes in post-MI patients are reproduced in simulations and explained by identified factors of ionic remodelling, with a weak signature in the resting LVEF. 1) T-wave inversion, Brugada phenocopy, and QT prolongation at the acute stage were explained by reversed transmural dispersion of repolarisation in the border zone and infarct, activation failure in the border zone, and increased repolarisation time in the border zone, respectively. 2) Large T-wave duration and amplitude at chronic stage reflects large repolarisation dispersion between remote and border zones, and global QT prolongation was caused by AP prolongation in the remote zone. 3) Reduction in LVEF is ubiquitous across acute and chronic post-MI phenotypes and can be explained by decreased intracellular calcium amplitude and activation failure (in the case of Brugada phenocopy). This effect was independent of changes in the dispersion of repolarisation. 4) Interestingly, fast pacing simulations with T-wave alternans or abnormal propagation driven by cellular alternans or EADs both showed preserved LVEF at resting heart rate, highlighting the fact that preserved LVEF at rest does not guarantee low arrhythmic risk.

Acute stage T-wave inversion and Brugada phenocopy are caused by reversed transmural repolarization gradient and regional conduction abnormality

Three distinct types of T-wave morphology were generated by our acute stage biventricular simulations: T-wave inversion, Brugada-phenocopy and normal upright T-wave. We obtained them by applying three types of acute BZs, considering both APD prolongation and shortening, as a reflection of the variable experimental results[14]. Collectively, our results

highlighted the importance of considering experimental variations in mimicking the inter-subject variability in patients. T-wave inversion is a commonly observed feature in the acute stage of post-MI patients, and is commonly associated with arrhythmic risk [68]. Here we showed the reversed transmural repolarisation gradient caused by APD prolongation in the epicardial BZ accounted for this phenotype. The link between transmural repolarisation gradient and T-wave polarity has been reported previously[69] and is consistent with our results. Brugada-phenocopy was also observed in some acute MI patients[60,70], and our simulation results showed it could be a reflection of regional conduction abnormality combined with APD prolongation. Although some animal experiments showed acute stage BZ APD shortening[14], we showed the prolongation of BZ APD was underlying the QT prolongation, T-wave inversion and Brugada phenocopy in the leads facing the infarct, which is consistent with the QTc prolongation observed in the anterior leads of acute anterior infarction patients[13,71]. Apart from the above, normal T-waves and QT intervals were also commonly observed in patients post percutaneous coronary intervention, which can be reproduced when the post-MI repolarisation dispersion was small between BZ and NZ. T-wave inversion, Brugada phenocopy and QT prolongation occur in the leads facing the infarct can be useful biomarkers indicating bigger repolarisation dispersions in the acute stage post-MI.

Wide and tall T-wave is explained by large repolarisation dispersions between BZ and RZ in healed post-MI hearts

Our simulated chronic ECGs recapitulated the recovery of T-wave polarity observed in patients after a period of healing. This was achieved through the recovery of the transmural

repolarisation gradient caused by the milder I_{Kr} inhibition in the chronic BZ[23]. Experimental studies in different species showed inconsistent results regarding the BZ APD[14]. Our chronic BZ remodelling produced slightly longer APD than the NZ, which is consistent with observations in healed human BZ[72]. However, in minipigs, these remodelling caused shorter BZ APD than in NZ[23]. This interesting discrepancy between minipigs and human may be due to the different balance of ionic currents across species, which showed the benefits of human electrophysiology models in overcoming the inter-species differences.

The two types of T-wave morphologies in the simulated chronic ECGs corresponded to different extents of RZ APD prolongations, which were commonly observed in healed RZ of post-MI animals[23], and in failing human myocytes[49,73]. The substantial RZ APD prolongation was reflected as global QT prolongation in all leads, and the large APD dispersion between chronic BZ and RZ generated wide and tall T-waves in the precordial leads facing the infarct. Previous simulation studies also found the T-wave amplitude and area were proportional to the dispersion of repolarisation[74,75]. Therefore, these results demonstrated that in patients with global QT prolongation, leads with bigger T-wave amplitudes could reflect increased local heterogeneity in repolarisation.

Post-MI ionic remodelling promoted repolarisation abnormalities, such as EADs and alternans

In addition to the enlarged APD dispersion between BZ and the surrounding tissue, the generation of repolarisation abnormalities can also increase the intra-ventricular electrophysiological heterogeneity, facilitating the generation of re-entrant waves. Two types of repolarisation abnormalities were observed in our post-MI models: EADs and alternans.

Post-MI ionic remodelling promoted alternans generation, which can be manifested as T-wave alternans in simulated ECGs, consistent with the higher incidence of T-wave alternans reported in post-MI patients[76]. One crucial factor promoting alternans behaviour is the increased activity of CaMKII, observed in the acute stage BZ[42], as well as in the hypertrophied and failing myocardium[77]. Enhanced CaMKII phosphorylation may preserve the contractility of the heart through the phosphorylation of phospholamban and the L-type calcium channels, but increased RyR phosphorylation by CaMKII resulted in prolonged RyR opening as well as the enhancement of spontaneous calcium sparks, which can contribute to alternans and triggered arrhythmias[58].

Generation of EADs due to chronic post-MI ionic remodelling, such as I_{Kr} inhibition and I_{NaL} enhancement, was consistent with previous studies[40]. EADs in the RZ can create large repolarisation dispersion in the ventricle, facilitating abnormal electrotonic wave propagations. Similar re-entrant waves caused by electrotonic gradients were also observed in previous studies of acute ischemia[78].

LVEF should be combined with QT and T-wave characteristics for arrhythmic risk stratification

In this study, we observed reductions of LVEF in the both the acute and the chronic post-MI stages. At both stages, ventricles with different extents of repolarisation dispersion may have similar LVEF because they have similar degrees of calcium reduction (acute stage T-wave inversion vs normal ST-T, and chronic stage two cases). Models with inducibility of T-wave alternans and arrhythmia at fast pacing rates may present with a preserved LVEF at resting heart rates (Figure 6-7). Our cellular level results also showed models with inducibility of

repolarisation abnormalities, such as alternans and EADs, tended to have more preserved CaT magnitudes at rest rates. Therefore, these phenomena all support the fact that preserved LVEF measured at rest does not guarantee low arrhythmic risk.

A recent clinical study of post-MI patients with preserved LVEF showed defibrillators are needed in those patients with electrophysiological risk factors, such as prolonged QTc, increased T-wave alternans, to prevent sudden cardiac death[79]. Consistently, we also found post-MI alternans and EADs can present as alternans of T-wave morphology and prolonged QT intervals. In addition to the global ECG changes, our simulation results also showed increased local repolarisation dispersion can be reflected in the leads facing the infarct: inverted T-wave and prolonged QT in the acute stage, and wide and tall T-wave in the chronic stage. Therefore, we suggest the consideration of these signs as markers of high arrhythmic risk.

Limitations

The main goal of this study is to investigate how varying degrees of ionic current remodelling can explain the phenotypic variability in ECG and LVEF biomarkers, therefore we did not introduce the effect of structural and geometric remodelling. The LVEF reduction in clinical cases can be more significant if a hypertrophied geometry is used instead of a control geometry and the RZ myocardium stiffness is increased to include post-MI diffuse fibrosis, or if reduced contractile function in the BZ is taken into account, such as shown in Supplementary Materials Figure S5 where the LVEF decreased more significantly when the BZ contractile function is completely turned off. In addition, post-MI ionic remodelling can be modulated by other acute and chronic factors such as autonomic modulation,

inflammation, cell death, and metabolic remodelling, which can be explored in future work. The limitations in this study call for a need for personalised digital twins to be generated in the future to facilitate a better understanding of the interaction between structural remodelling and electrophysiological alterations.

CONCLUSIONS

We demonstrated mechanisms underlying T-wave inversion, Brugada phenocopy, and upright T-wave in the acute post-MI stage, as well as the upright T-wave with a range of height and durations in the healed chronic stage. Our results show that T-wave inversion, wide and tall T-wave, and QT prolongation in the leads facing the infarct are indicative of local dispersion of repolarisation, which is independent from the reduction of LVEF. Our simulation results suggest the utilization of T-wave morphology, T-wave alternans and QT prolongation to improve risk stratification biomarkers even when the resting LVEF is preserved.

FUNDING

This work was supported by a Wellcome Trust Fellowship in Basic Biomedical Sciences to B.R. (214290/Z/18/Z), an Oxford-Bristol Myers Squibb Fellowship to X.Z. (R39207/CN063), the Personalised In-Silico Cardiology (PIC) project, the CompBioMed 1 and 2 Centre of Excellence in Computational Biomedicine (European Commission Horizon 2020 research and innovation programme, grant agreements No. 675451 and No. 823712), an NC3Rs Infrastructure for Impact Award (NC/P001076/ 1), the TransQST project (Innovative Medicines Initiative 2 Joint Undertaking under grant agreement No 116030, receiving

support from the European Union's Horizon 2020 research and innovation programme and EFPIA), and the Oxford BHF Centre of Research Excellence (RE/13/1/30181).

ACKNOWLEDGEMENTS

The authors would like to acknowledge Dr Erica Dall'Armellina, Dr Arka Das, and Dr Chris Kelly for providing the clinical ECG examples, and Dr Lei Wang, for discussions on the study.

DATA AVAILABILITY STATEMENT

The simulation input files and Alya executable required to replicate the simulated results will be made available upon request.

DECLARATION OF HELSINKI

The study complied with the Declaration of Helsinki, and informed consent has been obtained from the subjects.

REFERENCES

1. Elayi CS, Charnigo RJ, Heron PM, Lee BK, Olgin JE. Primary Prevention of Sudden Cardiac Death Early Post-Myocardial Infarction: Root Cause Analysis for Implantable Cardioverter-Defibrillator Failure and Currently Available Options. *Circ Arrhythm Electrophysiol* 2017;**10**.

2. Vazquez R, Bayes-Genis A, Cygankiewicz I, Pascual-Figal D, Grigorian-Shamagian L, Pavon R, Gonzalez-Juanatey JR, Cubero JM, Pastor L, Ordonez-Llanos J, Cinca J, Luna AB de, MUSIC Investigators. The MUSIC Risk score: a simple method for predicting mortality in ambulatory patients with chronic heart failure. *Eur Heart J* 2009;**30**:1088–1096.

3. Solomon SD, Zelenkofske S, McMurray JJV, Finn PV, Velazquez E, Ertl G, Harsanyi A, Rouleau JL, Maggioni A, Kober L, White H, Van de Werf F, Pieper K, Califf RM, Pfeffer MA, Valsartan in Acute Myocardial Infarction Trial (VALIANT) Investigators. Sudden death in patients with myocardial infarction and left ventricular dysfunction, heart failure, or both. *N Engl J Med* 2005;**352**:2581–2588.

4. Priori SG, Blomström-Lundqvist C, Mazzanti A, Blom N, Borggrefe M, Camm J, Elliott PM, Fitzsimons D, Hatala R, Hindricks G, Kirchhof P, Kjeldsen K, Kuck K-H, Hernandez-Madrid A, Nikolaou N, Norekvål TM, Spaulding C, Van Veldhuisen DJ, ESC Scientific Document Group. 2015 ESC Guidelines for the management of patients with ventricular arrhythmias and the prevention of sudden cardiac death: The Task Force for the Management of Patients with Ventricular Arrhythmias and the Prevention of Sudden Cardiac Death of the European Society of Cardiology (ESC). Endorsed by:

Association for European Paediatric and Congenital Cardiology (AEPC). *Eur Heart J* 2015;**36**:2793–2867.

5. Vaduganathan M, Claggett BL, Chatterjee NA, Anand IS, Sweitzer NK, Fang JC, O'Meara E, Shah SJ, Hegde SM, Desai AS, Lewis EF, Rouleau J, Pitt B, Pfeffer MA, Solomon SD. Sudden Death in Heart Failure With Preserved Ejection Fraction: A Competing Risks Analysis From the TOPCAT Trial. *JACC Heart Fail* 2018;**6**:653–661.

6. Ahnve S. QT interval prolongation in acute myocardial infarction. *Eur Heart J* 1985;**6 Suppl D**:85–95.

7. Oikarinen L, Viitasalo M, Toivonen L. Dispersions of the QT interval in postmyocardial infarction patients presenting with ventricular tachycardia or with ventricular fibrillation. *Am J Cardiol* 1998;**81**:694–697.

8. Spargias KS, Lindsay SJ, Kawar GI, Greenwood DC, Cowan JC, Ball SG, Hall AS. QT dispersion as a predictor of long-term mortality in patients with acute myocardial infarction and clinical evidence of heart failure. *Eur Heart J* 1999;**20**:1158–1165.

9. Shenthar J, Deora S, Rai M, Nanjappa Manjunath C. Prolonged Tpeak-end and Tpeak-end/QT ratio as predictors of malignant ventricular arrhythmias in the acute phase of ST-segment elevation myocardial infarction: a prospective case-control study. *Heart Rhythm* 2015;**12**:484–489.

10. Bloomfield DM, Steinman RC, Namerow PB, Parides M, Davidenko J, Kaufman ES, Shinn T, Curtis A, Fontaine J, Holmes D, Russo A, Tang C, Bigger JT. Microvolt T-wave alternans distinguishes between patients likely and patients not likely to benefit from

implanted cardiac defibrillator therapy: a solution to the Multicenter Automatic Defibrillator Implantation Trial (MADIT) II conundrum. *Circulation* 2004;**110**:1885–1889.

11. Al-Khatib SM, Stevenson WG, Ackerman MJ, Bryant WJ, Callans DJ, Curtis AB, Deal BJ, Dickfeld T, Field ME, Fonarow GC, Gillis AM, Granger CB, Hammill SC, Hlatky MA, Joglar JA, Kay GN, Matlock DD, Myerburg RJ, Page RL. 2017 AHA/ACC/HRS Guideline for Management of Patients With Ventricular Arrhythmias and the Prevention of Sudden Cardiac Death: A Report of the American College of Cardiology/American Heart Association Task Force on Clinical Practice Guidelines and the Heart Rhythm Society. *Circulation* 2018;**138**:e272–e391.

12. Doroghazi RM, Childers R. Time-related changes in the Q-T interval in acute myocardial infarction: possible relation to local hypocalcemia. *Am J Cardiol* 1978;**41**:684–688.

13. Cinca J, Figueras J, Tenorio L, Valle V, Trenchs J, Segura R, Rius J. Time course and rate dependence of Q-T interval changes during noncomplicated acute transmural myocardial infarction in human beings. *Am J Cardiol* 1981;**48**:1023–1028.

14. Mendonca Costa C, Plank G, Rinaldi CA, Niederer SA, Bishop MJ. Modeling the Electrophysiological Properties of the Infarct Border Zone. *Front Physiol* 2018;**9**.

15. Dun W, Baba S, Yagi T, Boyden PA. Dynamic remodeling of K+ and Ca2+ currents in cells that survived in the epicardial border zone of canine healed infarcted heart. *Am J Physiol Heart Circ Physiol* 2004;**287**:H1046-1054.

16. Aggarwal Rajesh, Boyden Penelope A. Diminished Ca2+ and Ba2+ Currents in Myocytes Surviving in the Epicardial Border Zone of the 5-Day Infarcted Canine Heart. *Circulation Research* 1995;**77**:1180–1191.

17. Jiang M, Cabo C, Yao J, Boyden PA, Tseng G. Delayed rectifier K currents have reduced amplitudes and altered kinetics in myocytes from infarcted canine ventricle. *Cardiovasc Res* 2000;**48**:34–43.

18. Hund TJ, Decker KF, Kanter E, Mohler PJ, Boyden PA, Schuessler RB, Yamada KA, Rudy Y. Role of activated CaMKII in abnormal calcium homeostasis and I(Na) remodeling after myocardial infarction: insights from mathematical modeling. *J Mol Cell Cardiol* 2008;**45**:420–428.

19. Yao J-A, Hussain W, Patel P, Peters NS, Boyden PA, Wit AL. Remodeling of gap junctional channel function in epicardial border zone of healing canine infarcts. *Circ Res* 2003;**92**:437–443.

20. Cabo C, Yao J, Boyden PA, Chen S, Hussain W, Duffy HS, Ciaccio EJ, Peters NS, Wit AL. Heterogeneous gap junction remodeling in reentrant circuits in the epicardial border zone of the healing canine infarct. *Cardiovasc Res* 2006;**72**:241–249.

21. Gardner PI, Ursell PC, Fenoglio JJ, Wit AL. Electrophysiologic and anatomic basis for fractionated electrograms recorded from healed myocardial infarcts. *Circulation* 1985;**72**:596–611.

22. Ursell PC, Gardner PI, Albala A, Fenoglio JJ, Wit AL. Structural and electrophysiological changes in the epicardial border zone of canine myocardial infarcts during infarct healing. *Circ Res* 1985;**56**:436–451.

23. Hegyi B, Bossuyt J, Griffiths LG, Shimkunas R, Coulibaly Z, Jian Z, Grimsrud KN, Sondergaard CS, Ginsburg KS, Chiamvimonvat N, Belardinelli L, Varró A, Papp JG, Pollesello P, Levijoki J, Izu LT, Boyd WD, Bányász T, Bers DM, Chen-Izu Y. Complex electrophysiological remodeling in postinfarction ischemic heart failure. *Proc Natl Acad Sci USA* 2018;**115**:E3036–E3044.

24. Pogwizd SM, Hoyt RH, Saffitz JE, Corr PB, Cox JL, Cain ME. Reentrant and focal mechanisms underlying ventricular tachycardia in the human heart. *Circulation* 1992;**86**:1872–1887.

25. Arevalo HJ, Vadakkumpadan F, Guallar E, Jebb A, Malamas P, Wu KC, Trayanova NA. Arrhythmia risk stratification of patients after myocardial infarction using personalized heart models. *Nat Commun* 2016;**7**.

26. Sack KL, Davies NH, Guccione JM, Franz T. Personalised computational cardiology: Patient-specific modelling in cardiac mechanics and biomaterial injection therapies for myocardial infarction. *Heart Fail Rev* 2016;**21**:815–826.

27. Wenk JF, Klepach D, Lee LC, Zhang Z, Ge L, Tseng EE, Martin A, Kozerke S, Gorman JH, Gorman RC, Guccione JM. First Evidence of Depressed Contractility in the Border Zone of a Human Myocardial Infarction. *The Annals of Thoracic Surgery* 2012;**93**:1188–1193.

28. Wang ZJ, Santiago A, Zhou X, Wang L, Margara F, Levrero-Florencio F, Das A, Kelly C, Dall'Armellina E, Vazquez M, Rodriguez B. Human biventricular electromechanical simulations on the progression of electrocardiographic and mechanical abnormalities in post-myocardial infarction. *Europace* 2021;**23**:i143–i152.

29. Streeter DD, Vaishnav RN, Patel DJ, Spotnitz HM, Ross J, Sonnenblick EH. Stress distribution in the canine left ventricle during diastole and systole. *Biophys J* 1970;**10**:345–363.

30. Mincholé A, Zacur E, Ariga R, Grau V, Rodriguez B. MRI-Based Computational Torso/Biventricular Multiscale Models to Investigate the Impact of Anatomical Variability on the ECG QRS Complex. *Front Physiol* 2019;**10**:1103.

31. Caldwell BJ, Trew ML, Sands GB, Hooks DA, LeGrice IJ, Smaill BH. Three distinct directions of intramural activation reveal nonuniform side-to-side electrical coupling of ventricular myocytes. *Circ Arrhythm Electrophysiol* 2009;**2**:433–440.

32. Stone PH, Raabe DS, Jaffe AS, Gustafson N, Muller JE, Turi ZG, Rutherford JD, Poole WK, Passamani E, Willerson JT. Prognostic significance of location and type of myocardial infarction: independent adverse outcome associated with anterior location. *J Am Coll Cardiol* 1988;**11**:453–463.

33. Parker AB, Waller BF, Gering LE. Usefulness of the 12-lead electrocardiogram in detection of myocardial infarction: electrocardiographic-anatomic correlations--Part II. *Clin Cardiol* 1996;**19**:141–148.

34. Tomek J, Bueno-Orovio A, Passini E, Zhou X, Minchole A, Britton O, Bartolucci C, Severi S, Shrier A, Virag L, Varro A, Rodriguez B. Development, calibration, and validation of a novel human ventricular myocyte model in health, disease, and drug block. Faraldo-Gómez JD, Barkai N, Hund T, Maleckar M, eds. *eLife* 2019;**8**:e48890.

35. Land S, Park-Holohan S-J, Smith NP, Remedios CG dos, Kentish JC, Niederer SA. A model of cardiac contraction based on novel measurements of tension development in human cardiomyocytes. *Journal of Molecular and Cellular Cardiology* 2017;**106**:68–83.

36. Margara F, Wang ZJ, Levrero-Florencio F, Santiago A, Vázquez M, Bueno-Orovio A, Rodriguez B. In-silico human electro-mechanical ventricular modelling and simulation for drug-induced pro-arrhythmia and inotropic risk assessment. *Progress in Biophysics and Molecular Biology* 2021;**159**:58–74.

37. Sun K, Stander N, Jhun C-S, Zhang Z, Suzuki T, Wang G-Y, Saeed M, Wallace AW, Tseng EE, Baker AJ, Saloner D, Einstein DR, Ratcliffe MB, Guccione JM. A computationally efficient formal optimization of regional myocardial contractility in a sheep with left ventricular aneurysm. *J Biomech Eng* 2009;**131**:111001.

38. Passini E, Trovato C, Morissette P, Sannajust F, Bueno-Orovio A, Rodriguez B. Drug-induced shortening of the electromechanical window is an effective biomarker for in silico prediction of clinical risk of arrhythmias. *Br J Pharmacol* 2019;**176**:3819–3833.

39. Zhou X, Qu Y, Passini E, Bueno-Orovio A, Liu Y, Vargas HM, Rodriguez B. Blinded In Silico Drug Trial Reveals the Minimum Set of Ion Channels for Torsades de Pointes Risk Assessment. *Front Pharmacol* 2019;**10**:1643.

40. Coppini R, Ferrantini C, Yao L, Fan P, Del Lungo M, Stillitano F, Sartiani L, Tosi B, Suffredini S, Tesi C, Yacoub M, Olivotto I, Belardinelli L, Poggesi C, Cerbai E, Mugelli A. Late sodium current inhibition reverses electromechanical dysfunction in human hypertrophic cardiomyopathy. *Circulation* 2013;**127**:575–584.

41. Britton OJ, Bueno-Orovio A, Virág L, Varró A, Rodriguez B. The Electrogenic Na(+)/K(+) Pump Is a Key Determinant of Repolarization Abnormality Susceptibility in Human Ventricular Cardiomyocytes: A Population-Based Simulation Study. *Front Physiol* 2017;**8**:278.

42. Hund TJ, Decker KF, Kanter E, Mohler PJ, Boyden PA, Schuessler RB, Yamada KA, Rudy Y. Role of activated CaMKII in abnormal calcium homeostasis and I(Na) remodeling after myocardial infarction: insights from mathematical modeling. *J Mol Cell Cardiol* 2008;**45**:420–428.

43. Decker KF, Rudy Y. Ionic mechanisms of electrophysiological heterogeneity and conduction block in the infarct border zone. *Am J Physiol Heart Circ Physiol* 2010;**299**:H1588-1597.

44. Tomek J, Rodriguez B, Bub G, Heijman J. β-Adrenergic receptor stimulation inhibits proarrhythmic alternans in postinfarction border zone cardiomyocytes: a computational analysis. *Am J Physiol Heart Circ Physiol* 2017;**313**:H338–H353.

45. Chang P, Turker I, Lopshire JC, Masroor S, Nguyen B, Tao W, Rubart M, Chen P, Chen Z, Ai T. Heterogeneous Upregulation of Apamin□Sensitive Potassium Currents in Failing Human Ventricles. *J Am Heart Assoc* 2013;**2**.

46. Valdivia CR, Chu WW, Pu J, Foell JD, Haworth RA, Wolff MR, Kamp TJ, Makielski JC. Increased late sodium current in myocytes from a canine heart failure model and from failing human heart. *Journal of Molecular and Cellular Cardiology* 2005;**38**:475–483.

47. Jiang MT, Lokuta AJ, Farrell EF, Wolff MR, Haworth RA, Valdivia HH. Abnormal Ca2+ release, but normal ryanodine receptors, in canine and human heart failure. *Circ Res* 2002;**91**:1015–1022.

48. Maltsev VA, Silverman N, Sabbah HN, Undrovinas AI. Chronic Heart Failure Slows Late Sodium Current in Human and Canine Ventricular Myocytes: Implications for Repolarization Variability. *European journal of heart failure* 2007;**9**:219.

49. Li G-R, Lau C-P, Leung T-K, Nattel S. Ionic current abnormalities associated with prolonged action potentials in cardiomyocytes from diseased human right ventricles. *Heart Rhythm* 2004;**1**:460–468.

50. Zicha S, Xiao L, Stafford S, Cha TJ, Han W, Varro A, Nattel S. Transmural expression of transient outward potassium current subunits in normal and failing canine and human hearts. *J Physiol (Lond)* 2004;**561**:735–748.

51. Holzem Katherine M, Glukhov Alexey V, Efimov Igor R. Abstract 16014: The Role of IKr in Transmural Repolarization Abnormalities in Human Heart Failure. *Circulation* 2011;**124**:A16014–A16014.

52. Schwinger RH, Wang J, Frank K, Müller-Ehmsen J, Brixius K, McDonough AA, Erdmann E. Reduced sodium pump alpha1, alpha3, and beta1-isoform protein levels and

Na+,K+-ATPase activity but unchanged Na+-Ca2+ exchanger protein levels in human heart failure. *Circulation* 1999;**99**:2105–2112.

53. Elshrif MM, Pengcheng Shi null, Cherry EM. Electrophysiological properties under heart failure conditions in a human ventricular cell: a modeling study. *Conf Proc IEEE Eng Med Biol Soc* 2014;**2014**:4324–4329.

54. Gomez JF, Cardona K, Romero L, Jr JMF, Trenor B. Electrophysiological and Structural Remodeling in Heart Failure Modulate Arrhythmogenesis. 1D Simulation Study. *PLOS ONE* 2014;**9**:e106602.

55. Høydal MA, Kirkeby-Garstad I, Karevold A, Wiseth R, Haaverstad R, Wahba A, Stølen TL, Contu R, Condorelli G, Ellingsen Ø, Smith GL, Kemi OJ, Wisløff U. Human cardiomyocyte calcium handling and transverse tubules in mid-stage of post-myocardial-infarction heart failure. *ESC Heart Fail* 2018;**5**:332–342.

56. Hegyi B, Bossuyt J, Griffiths LG, Shimkunas R, Coulibaly Z, Jian Z, Grimsrud KN, Sondergaard CS, Ginsburg KS, Chiamvimonvat N, Belardinelli L, Varró A, Papp JG, Pollesello P, Levijoki J, Izu LT, Boyd WD, Bányász T, Bers DM, Chen-Izu Y. Complex electrophysiological remodeling in postinfarction ischemic heart failure. *Proc Natl Acad Sci USA* 2018;**115**:E3036–E3044.

57. Hoch B, Meyer R, Hetzer R, Krause EG, Karczewski P. Identification and expression of delta-isoforms of the multifunctional Ca2+/calmodulin-dependent protein kinase in failing and nonfailing human myocardium. *Circ Res* 1999;**84**:713–721.

58. Maier LS, Bers DM. Role of Ca2+/calmodulin-dependent protein kinase (CaMK) in excitation-contraction coupling in the heart. *Cardiovasc Res* 2007;**73**:631–640.

59. Santiago A, Aguado-Sierra J, Zavala-Aké M, Doste-Beltran R, Gómez S, Arís R, Cajas JC, Casoni E, Vázquez M. Fully coupled fluid-electro-mechanical model of the human heart for supercomputers. *Int J Numer Method Biomed Eng* 2018;**34**:e3140.

60. Anselm DD, Evans JM, Baranchuk A. Brugada phenocopy: A new electrocardiogram phenomenon. *World J Cardiol* 2014;**6**:81–86.

61. Bousseljot R, Kreiseler D, Schnabel A. Nutzung der EKG-Signaldatenbank CARDIODAT der PTB über das Internet. *Biomedizinische Technik/Biomedical Engineering* 2009:317–318.

62. Goldberger AL, Amaral LA, Glass L, Hausdorff JM, Ivanov PC, Mark RG, Mietus JE, Moody GB, Peng CK, Stanley HE. PhysioBank, PhysioToolkit, and PhysioNet: components of a new research resource for complex physiologic signals. *Circulation* 2000;**101**:E215-220.

63. Zhou X, Bueno-Orovio A, Orini M, Hanson B, Hayward M, Taggart P, Lambiase PD, Burrage K, Rodriguez B. In Vivo and In Silico Investigation Into Mechanisms of Frequency Dependence of Repolarization Alternans in Human Ventricular Cardiomyocytes. *Circ Res* 2016;**118**:266–278.

64. Tomek J, Tomková M, Zhou X, Bub G, Rodriguez B. Modulation of Cardiac Alternans by Altered Sarcoplasmic Reticulum Calcium Release: A Simulation Study. *Front Physiol* 2018;**9**.

65. Livshitz LM, Rudy Y. Regulation of Ca2+ and electrical alternans in cardiac myocytes: role of CAMKII and repolarizing currents. *Am J Physiol Heart Circ Physiol* 2007;**292**:H2854-2866.

66. Kameyama M, Hirayama Y, Saitoh H, Maruyama M, Atarashi H, Takano T. Possible contribution of the sarcoplasmic reticulum Ca(2+) pump function to electrical and mechanical alternans. *J Electrocardiol* 2003;**36**:125–135.

67. Ikeda T, Sakata T, Takami M, Kondo N, Tezuka N, Nakae T, Noro M, Enjoji Y, Abe R, Sugi K, Yamaguchi T. Combined assessment of T-wave alternans and late potentials used to predict arrhythmic events after myocardial infarction. A prospective study. *J Am Coll Cardiol* 2000;**35**:722–730.

68. Tikkanen JT, Kenttä T, Porthan K, Huikuri HV, Junttila MJ. Electrocardiographic T Wave Abnormalities and the Risk of Sudden Cardiac Death: The Finnish Perspective. *Ann Noninvasive Electrocardiol* 2015;**20**:526–533.

69. Okada J, Washio T, Maehara A, Momomura S, Sugiura S, Hisada T. Transmural and apicobasal gradients in repolarization contribute to T-wave genesis in human surface ECG. *American Journal of Physiology-Heart and Circulatory Physiology* 2011;**301**:H200–H208.

70. Ferrando□Castagnetto F, Garibaldi□Remuñan A, Vignolo G, Ricca□Mallada R, Baranchuk A. Brugada Phenocopy as a Dynamic Electrocardiographic Pattern during Acute Anterior Myocardial Infarction. *Ann Noninvasive Electrocardiol* 2016;**21**:425–428.

71. Guaricci AI, Carità P, Lorenzoni V, Casavecchia G, Rabbat M, Ieva R, Brunetti ND, Andreini D, Di Biase M, Marenzi G, Bartorelli A, Pepi M, Pontone G. QT-interval evaluation in primary percutaneous coronary intervention of ST-segment elevation myocardial infarction for prediction of myocardial salvage index. *PLoS One* 2018;**13**.

72. Dangman KH, Danilo P, Hordof AJ, Mary-Rabine L, Reder RF, Rosen MR. Electrophysiologic characteristics of human ventricular and Purkinje fibers. *Circulation* 1982;**65**:362–368.

73. Piacentino V, Weber CR, Chen X, Weisser-Thomas J, Margulies KB, Bers DM, Houser SR. Cellular basis of abnormal calcium transients of failing human ventricular myocytes. *Circ Res* 2003;**92**:651–658.

74. Arteyeva NV, Azarov JE. Effect of action potential duration on Tpeak-Tend interval, T-wave area and T-wave amplitude as indices of dispersion of repolarization: Theoretical and simulation study in the rabbit heart. *J Electrocardiol* 2017;**50**:919–924.

75. Van Huysduynen BH, Swenne CA, Draisma HHM, Antoni ML, Van De Vooren H, Van Der Wall EE, Schalij MJ. Validation of ECG indices of ventricular repolarization heterogeneity: a computer simulation study. *J Cardiovasc Electrophysiol* 2005;**16**:1097–1103.

76. Martin DT, Shoraki A, Nesto RW, Rutter MK. Influence of diabetes and/or myocardial infarction on prevalence of abnormal T-wave alternans. *Ann Noninvasive Electrocardiol* 2009;**14**:355–359.

77. Anderson ME, Brown JH, Bers DM. CaMKII in myocardial hypertrophy and heart failure. *J Mol Cell Cardiol* 2011;**51**:468–473.

78. Dutta S, Mincholé A, Zacur E, Quinn TA, Taggart P, Rodriguez B. Early afterdepolarizations promote transmural reentry in ischemic human ventricles with reduced repolarization reserve. *Prog Biophys Mol Biol* 2016;**120**:236–248.

79. Gatzoulis KA, Tsiachris D, Arsenos P, Antoniou C-K, Dilaveris P, Sideris S, Kanoupakis E, Simantirakis E, Korantzopoulos P, Goudevenos I, Flevari P, Iliodromitis E, Sideris A, Vassilikos V, Fragakis N, Trachanas K, Vernardos M, Konstantinou I, Tsimos K, Xenogiannis I, Vlachos K, Saplaouras A, Triantafyllou K, Kallikazaros I, Tousoulis D. Arrhythmic risk stratification in post-myocardial infarction patients with preserved ejection fraction: the PRESERVE EF study. *Eur Heart J* 2019;**40**:2940–2949.

FIGURE LEGENDS

Figure 1: Multi-scale modelling and simulation of post-myocardial infarction. (A) At whole-organ level, simulated clinical ECG and pressure volume biomarkers. (B) At biventricular level, the electrophysiological behaviour is modelled with a fast endocardial activation layer to approximate Purkinje-myocardial junction, with appropriate transmural and apico-basal heterogeneities in action potential duration, and transmurally varying myocyte orientation. The pumping behaviour is modelled by coupling the intraventricular pressures with a two-element Windkessel model of arterial haemodynamics with a fixed basal plane. (C) An anterior 75% transmural infarction is modelled with acute and chronic ionic remodellings embedded in the border zone and remote zones. Standard 12-lead ECG was evaluated at standard body-surface locations using the pseudo-ECG method. (D) The population of models of healthy (baseline) and acute and chronic post-MI remodelling were generated by varying ionic conductances of the ToR-ORd model (E) and applying remodelling from literature. (E) Electromechanically coupled cellular model, showing remodelled ionic currents for acute and chronic stages.

Figure 2: Simulated ECGs recapitulate clinical phenotypes in acute and chronic post-myocardial infarction (post-MI). (A) In acute stage post-MI, simulated ECGs show T-wave inversion (border zone model 1 (BZ1)), Brugada phenocopy (BZ2), and normal phenotypes (BZ3), in accordance with phenotypes found in clinical databases. (B) In chronic stage post-MI, simulated ECGs show prolonged QT and upright T-waves with a range of amplitude and duration (remote zone model 1 and 2 (RZ1, RZ2)) comparable to those observed in clinical databases.

Figure 3: Multi-scale electrophysiological mechanisms explaining ST and T-wave phenotypes in acute post-myocardial infarction. A) Whole-ventricular electromechanical simulations showing conduction delay in border zone (T-wave inversion and normal ST-T) and conduction block (Brugada phenocopy), as well as large repolarisation dispersion and altered transmural repolarisation gradient (T-wave inversion and Brugada phenocopy). Red in activation map show regions of no activation (NA), green in repolarisation map show regions of no repolarisation (NR). B) Cellular simulations in the border zone show action potential duration prolongation (T-wave inversion and Brugada phenocopy) and slight shortening (normal ST-T), with decreased calcium amplitude in all phenotypes, with a corresponding decrease in active tension generation. C) I_{Na}, I_{CaL}, and I_{Kr} remodelling underpin reduced conduction, reduced calcium amplitude, and alterations in action potential duration, respectively, in all acute phenotypes.

Figure 4: Multi-scale electrophysiological mechanisms explaining QT and T-wave phenotypes in chronic post-myocardial infarction. A) Whole-ventricular electromechanical simulations showing conduction delay in border zone (slight QT prolongation and large T-wave), as well as large repolarisation dispersion (large T-wave). Red in activation map show regions of no activation (NA), green in repolarisation map show regions of no repolarisation (NR). B) Cellular simulations in the border zone show varying degrees of action potential duration prolongation in the remote zone (RZ) corresponding to extent of QT prolongation, with decreased calcium amplitude in remote and border zone of

both phenotypes, with corresponding decrease in active tension generation. C) As in acute stage, I_{Na}, I_{CaL}, and I_{Kr} remodelling underpin reduced conduction, reduced calcium amplitude, and degree of prolongation in action potential duration, respectively, in both chronic phenotypes.

Figure 5: Simulations for both acute and chronic post-myocardial show reduced LVEF and heterogeneous systolic deformation. (A) Reduced LVEF in all acute phenotypes due to reduced active tension amplitude in the border zone (BZ1~3). Brugada phenocopy shows the lowest LVEF due to activation block and loss of contractile function in the border zone in addition to reduced active tension amplitude in the activated border zone due to ionic remodelling. Reduced contractile function in infarct and border zone results in infarct thinning and bulging in systole. Systolic cross section of control simulation shown in black (CTL) with post-MI cross-sections superimposed. (B) Reduced LVEF in both chronic phenotypes due to reduced active tension amplitude in remote zone (RZ) and border zones, independent of the extent of QT prolongation (RZ1, RZ2). Scar stiffening helped to reduce infarct bulging. Systolic cross-section of control simulation shown in black (CTL) with post-MI cross-sections superimposed.

Figure 6: Fast pacing shows alternans behaviour in single-cell simulation and ECG abnormalities and pressure fluctuations. (A) An epicardial population of models with remote zone 1 (RZ1) remodelling showing alternans, with 55 ms alternans magnitude in APD for the highlighted red trace. (B) A representative model was selected from a population of models with remote zone 2 (RZ) remodelling, where large action potential and

calcium transient alternans were caused by EADs in the midmyocardial cell type at 500 ms CL pacing. (C) Whole-ventricular simulations using the representative alternans cell model in the remote zone showed T-wave alternans at fast pacing, with preserved left ventricular ejection fraction (LVEF) at resting heart rate.

Figure 7: Alternans and EAD behaviour in single cells can be manifested as abnormal wave propagations in biventricular simulations with preserved LVEF at rest. (A) A population of models demonstrating chronic remote zone 2 (RZ2) remodelling in promoting EADs. A representative example was selected from the population of models that showed EAD caused by repolarisation failure. (B) Membrane potential changes for the first 1010 ms of fast pacing simulation, showing ectopic wave generation driven by electrotonic gradient at 710 ms, and anticlockwise propagation of ectopic wave from basal view starting at 810 ms. (C) Local action potential at anterior, lateral, posterior, and right ventricular sites. (D) Simulated ECGs showed prolonged QT and T-wave duration at resting heart rate with preserved LVEF, then at fast pacing, significant ECG abnormalities were observed.

Human Cardiac Multi-scale Electromechanical Modelling and Simulation

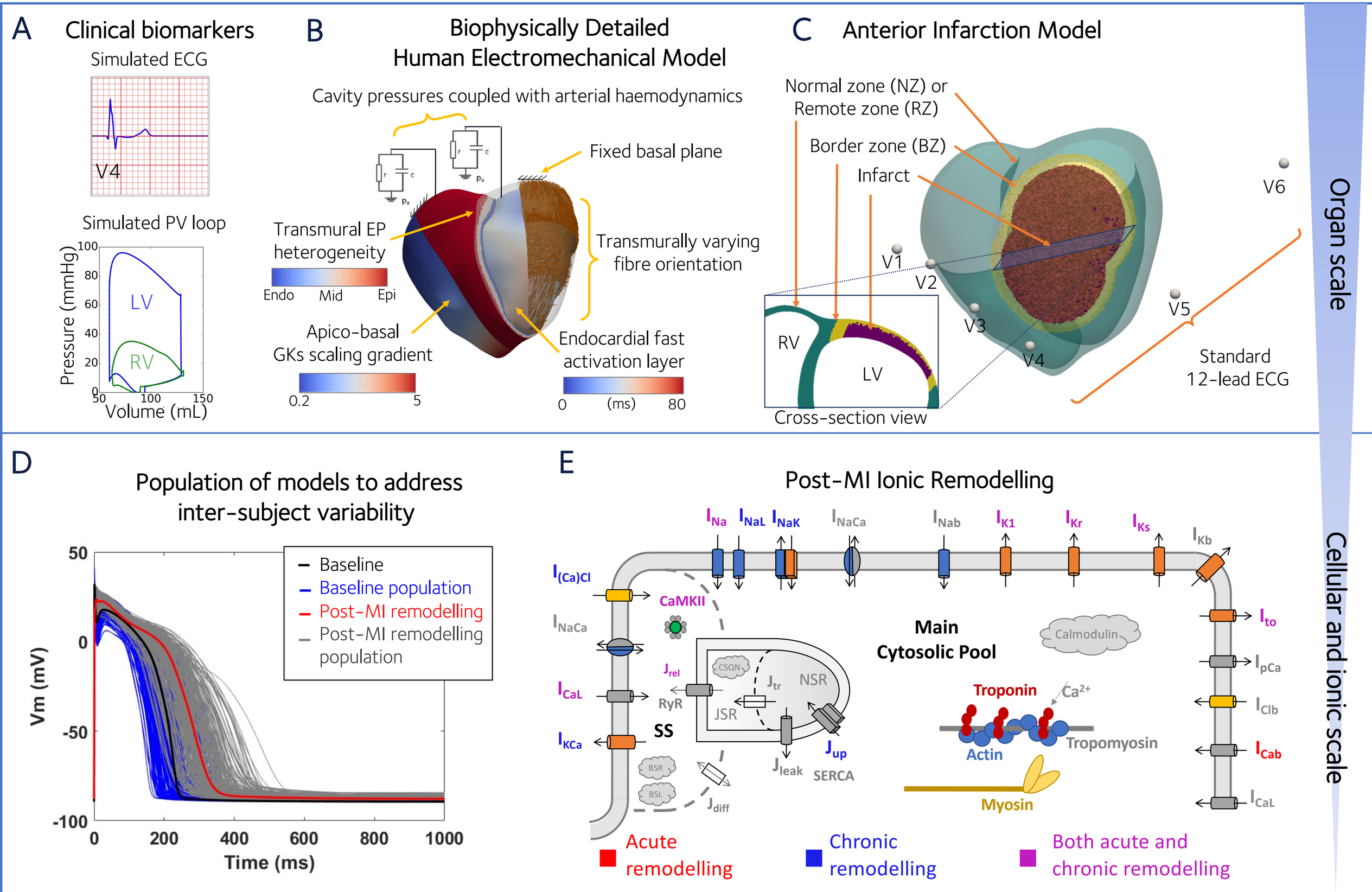

Simulated post-MI ECG phenotypes

A. Acute

	Control	T-wave inversion (BZ1)	Brugada phenocopy (BZ2)	Normal ST-T (BZ3)
QT interval:	317±8 ms	349±20 ms	362±21 ms	325±6 ms
Simulated ECG:	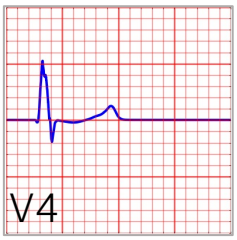	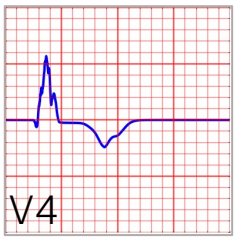	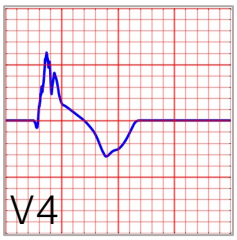	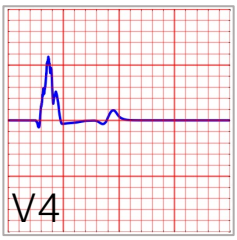
Clinical ECG:			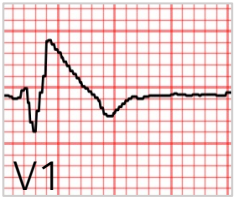	

B. Chronic

	Control	Slight QT prolongation (RZ1)	Large T-wave (RZ2)
Tpe duration:	57±11 ms	72±16 ms	162 ± 41 ms
QT interval:	317±8 ms	380±8 ms	565±10 ms
Simulated ECG:	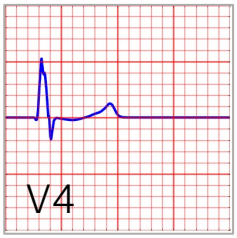		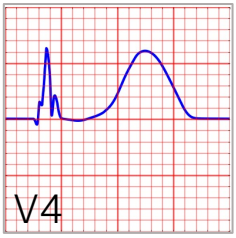
Clinical database ECG:			

Acute post-MI multi-scale mechanisms

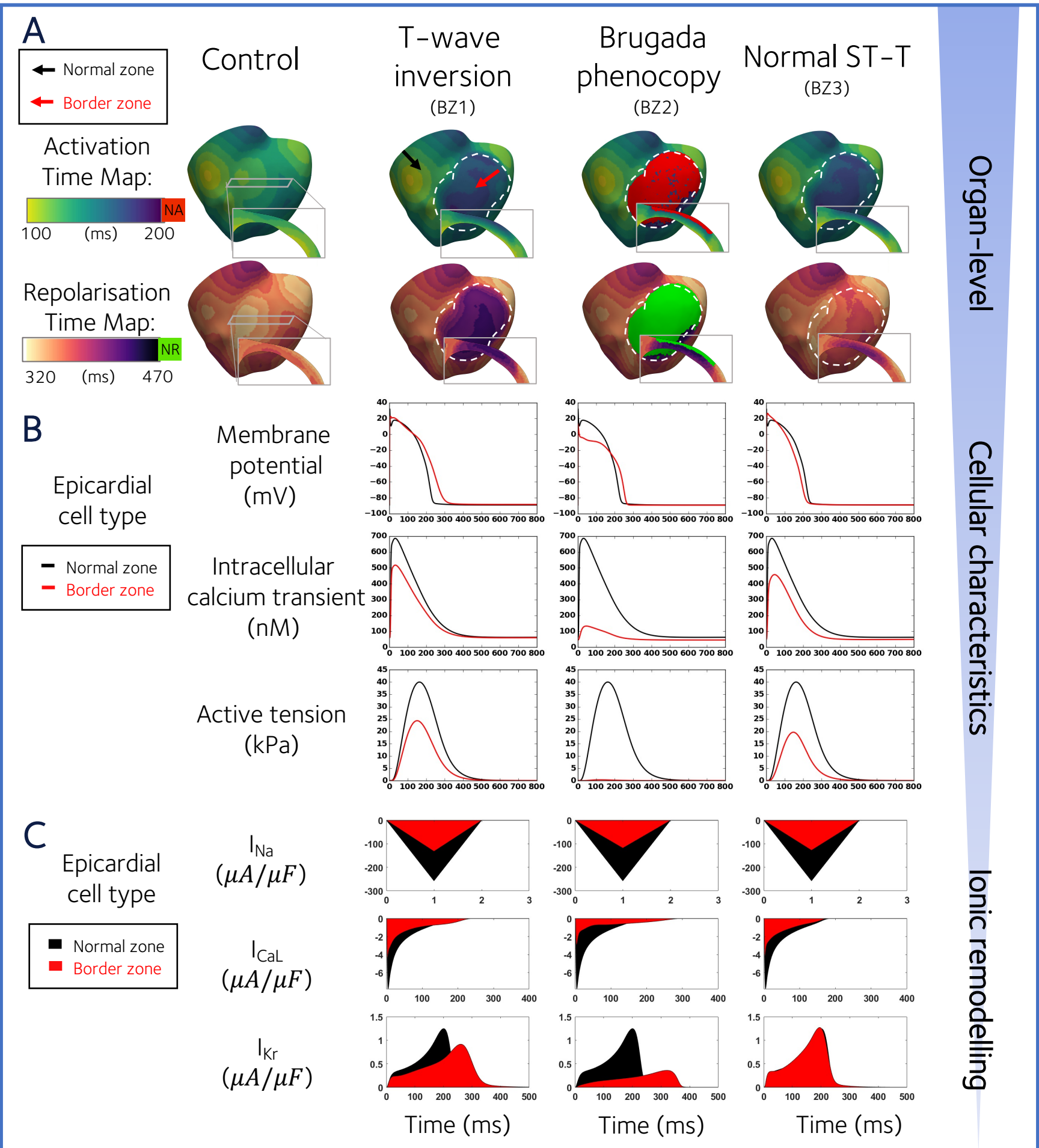

Chronic post-MI multi-scale mechanisms

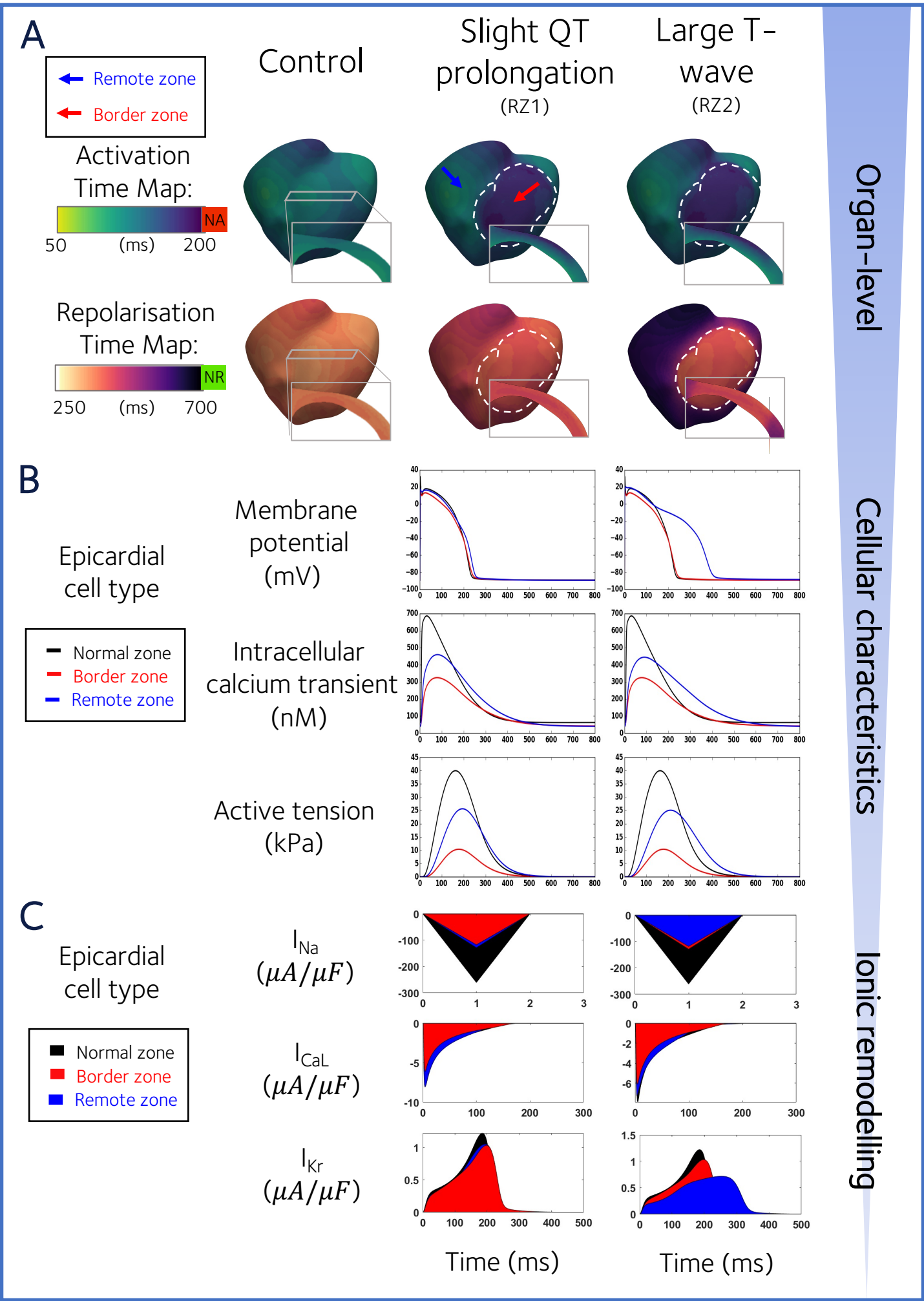

Effect of ionic remodelling on mechanical function

A. Acute

Biomarkers | Organ | Tissue | Cell

Control	T-wave inversion (BZ1)	Brugada phenocopy (BZ2)	Normal ST-T (BZ3)
LVEF: 53%	LVEF: 47%	LVEF: 43%	LVEF: 47%

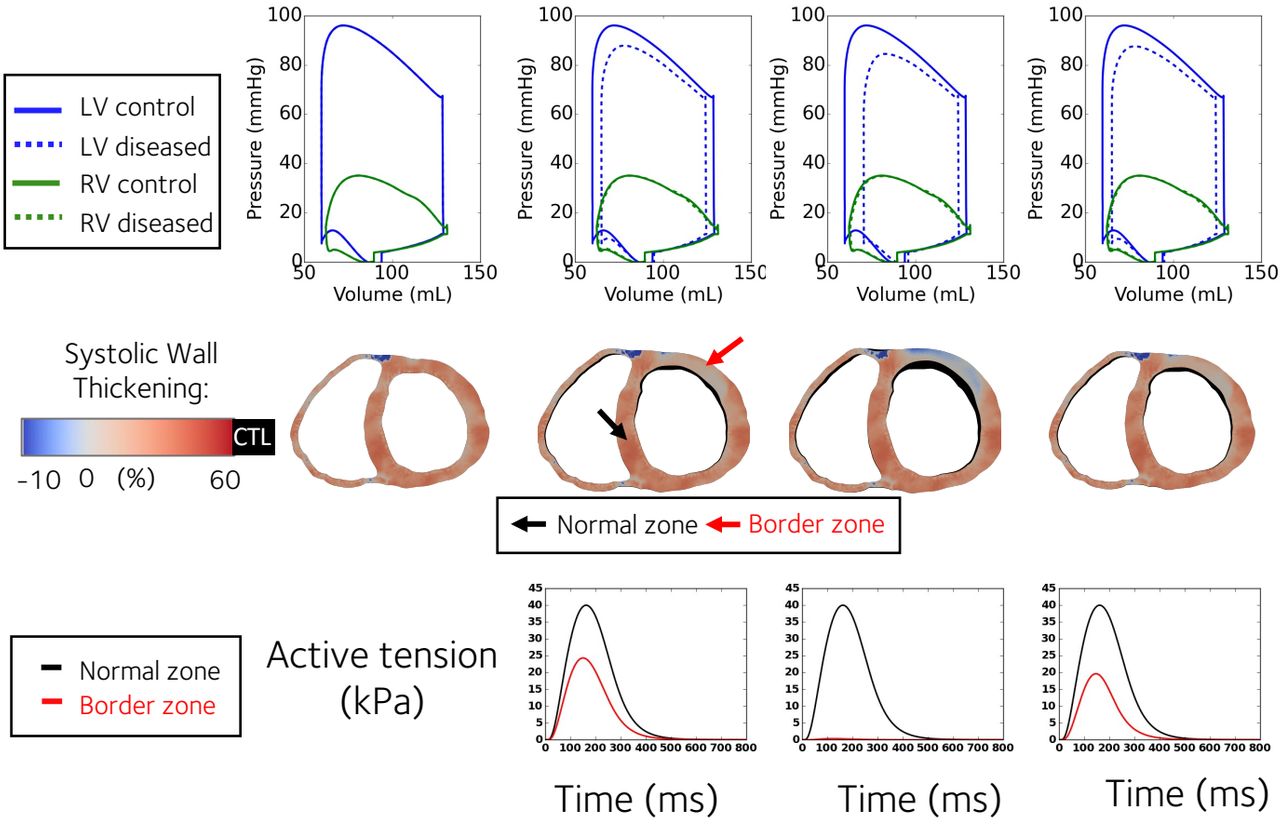

B. Chronic

Biomarkers | Organ | Tissue | Cell

	Control	Slight QT prolongation (RZ1)	Large T-wave (RZ2)
	LVEF: 53%	LVEF: 48%	LVEF: 48%
End diastolic volume:	128 mL	126 mL	126 mL
Peak systolic pressure:	12 kPa	11 kPa	11 kPa

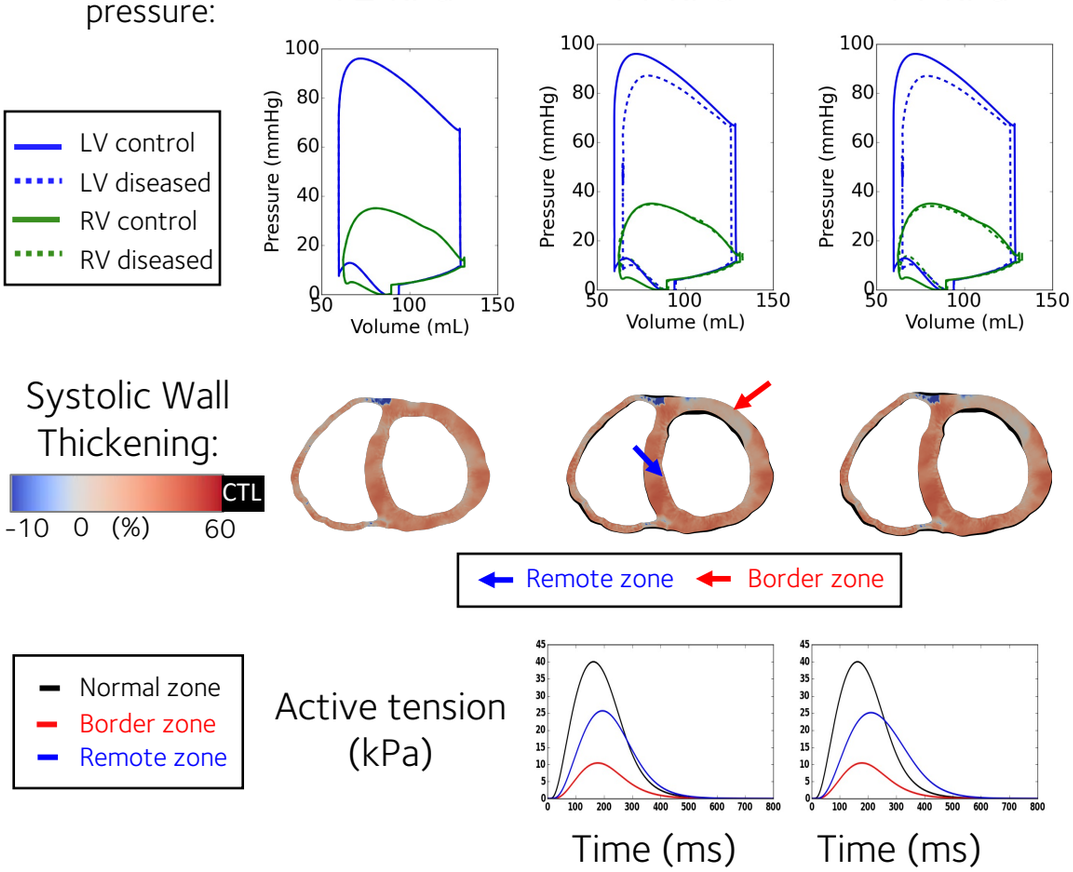

Post-MI T-wave Alternans Mechanisms

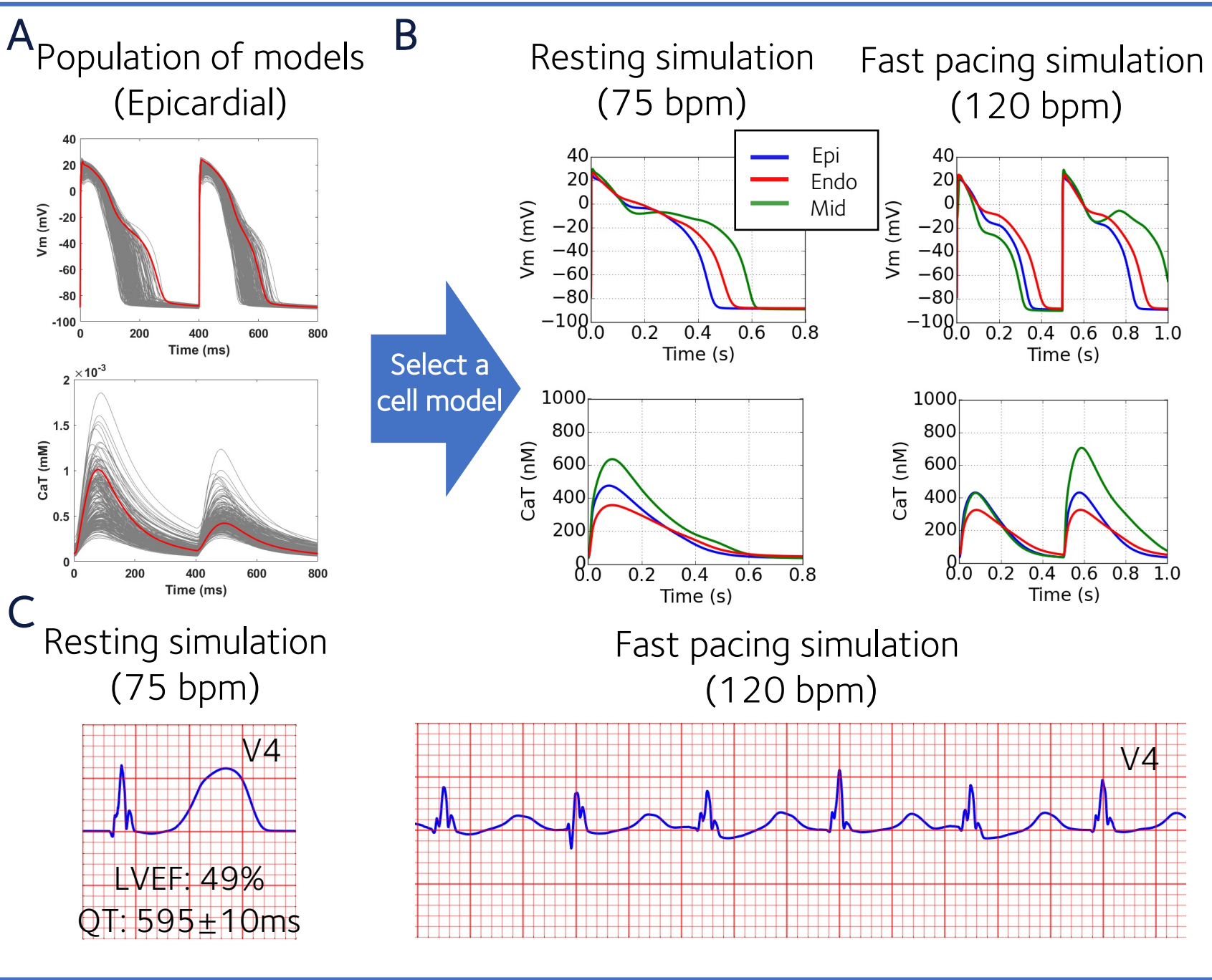

Post-MI Abnormal Electrical Wave Propagation Mechanisms

A. Cellular EADs

Population of models with chronic post-MI remodelling

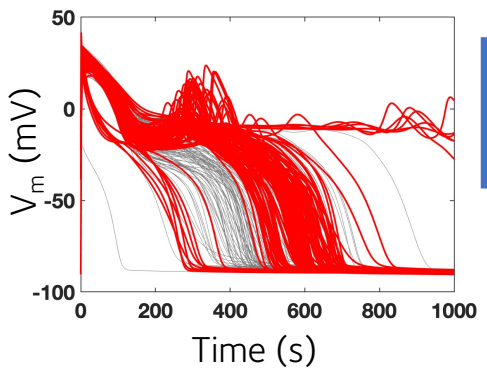

Select a cell model

Resting simulation (75 bpm)

Epi
Endo
Mid

Fast pacing simulation (120 bpm)

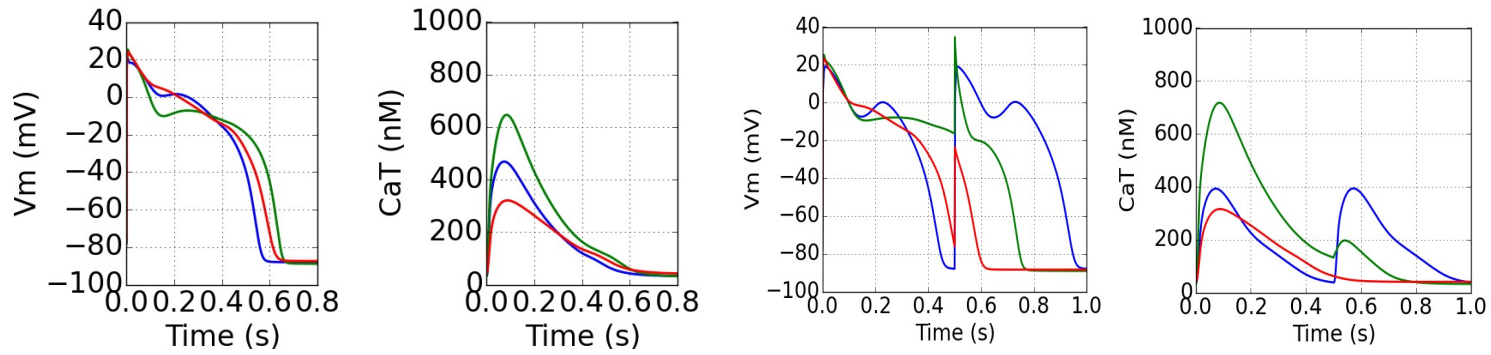

B. Ventricular-level wave propagation

610 ms | 710 ms | 810 ms | 910 ms | 1010 ms

Basal view

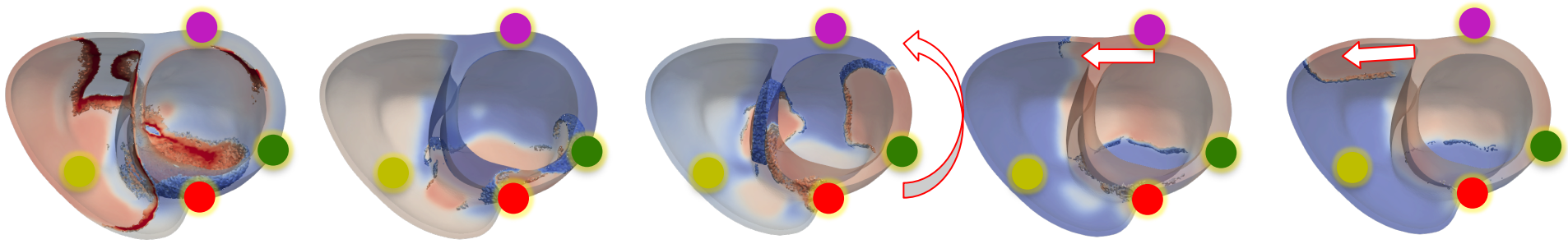

LV lateral view

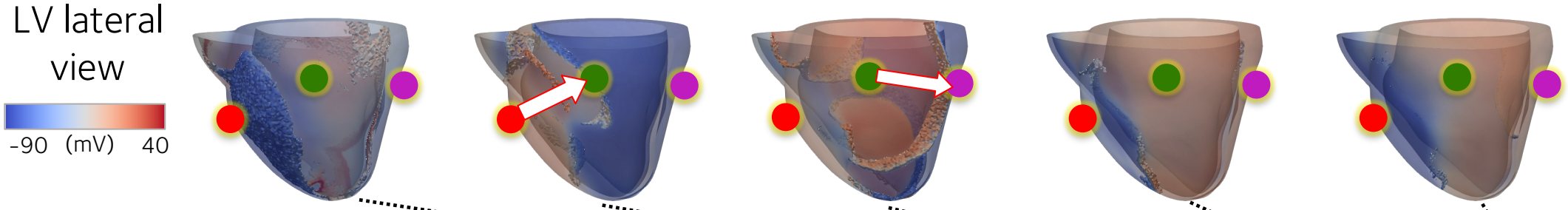

C. EADs in ventricles

- Sinus rhythm
- Anterior chronic BZ
- Lateral RZ
- Posterior RZ
- Right ventricular RZ

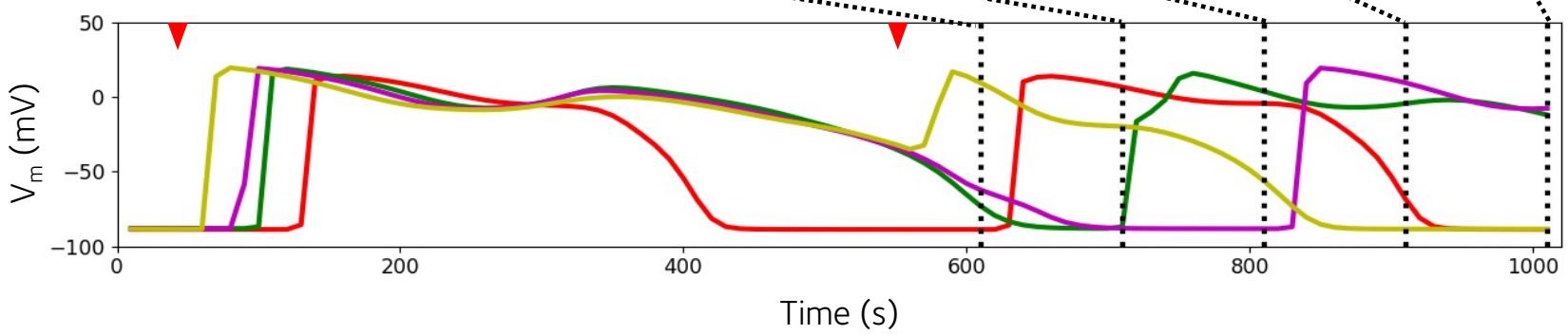

D. Simulated ECGs

Sinus rhythm

Resting simulation (75 bpm)

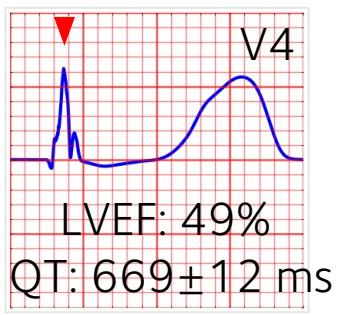

Fast pacing simulation (120 bpm)

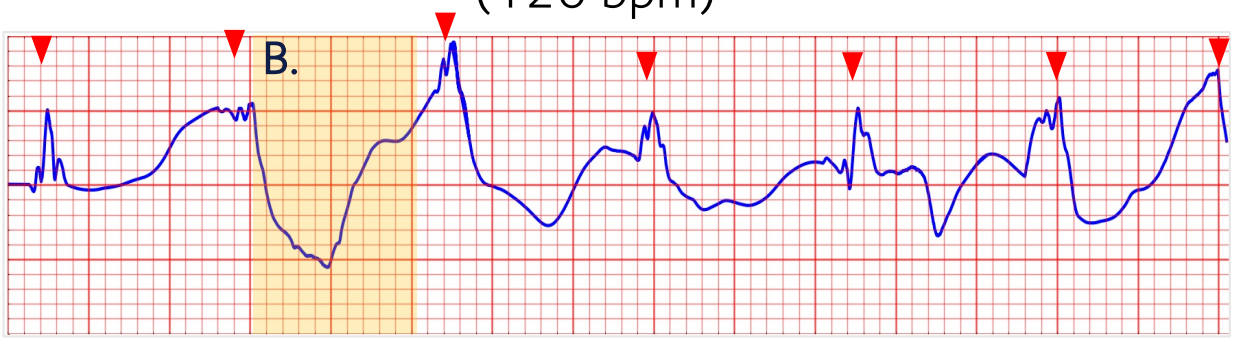

Cellular EADs

Organ-level effect

Simulated Clinical Biomarkers